Letter

Implications of pulsar timing array data for scalar-induced gravitational waves and primordial black holes: Primordial non-Gaussianity f_{NL} considered

Sai Wang,[1] Zhi-Chao Zhao,[2,*] Jun-Peng Li,[1,3] and Qing-Hua Zhu[4]

[1]*Theoretical Physics Division, Institute of High Energy Physics, Chinese Academy of Sciences, Beijing 100049, People's Republic of China*

[2]*Department of Applied Physics, College of Science, China Agricultural University, Qinghua East Road, Beijing 100083, People's Republic of China*

[3]*School of Physical Sciences, University of Chinese Academy of Sciences, Beijing 100049, People's Republic of China*

[4]*CAS Key Laboratory of Theoretical Physics, Institute of Theoretical Physics, Chinese Academy of Sciences, Beijing 100190, People's Republic of China*

(Received 28 September 2023; accepted 14 February 2024; published 15 March 2024)

Multiple pulsar-timing-array collaborations have reported strong evidence for the existence of a gravitational-wave background. We study physical implications of this signal for cosmology, assuming that it is attributed to scalar-induced gravitational waves. By incorporating primordial non-Gaussianity $f_{\rm NL}$, we specifically examine the nature of primordial curvature perturbations and primordial black holes. We find that the signal allows for a primordial non-Gaussianity $f_{\rm NL}$ in the range of $-4.1 \lesssim f_{\rm NL} \lesssim 4.1$ (68% confidence intervals) and a mass range for primordial black holes $m_{\rm pbh}$ spanning from $\sim 10^{-5} M_\odot$ to $\sim 10^{-2} M_\odot$. Furthermore, we find that the signal favors a negative non-Gaussianity, which can suppress the abundance of primordial black holes. We also demonstrate that the anisotropies of scalar-induced gravitational waves serve as a powerful tool to probe the non-Gaussianity $f_{\rm NL}$. We conduct a comprehensive analysis of the angular power spectrum within the nano-Hertz band. Looking ahead, we anticipate that future projects, such as the Square Kilometre Array, will have the potential to measure these anisotropies and provide further insights into the primordial universe.

DOI: 10.1103/PhysRevResearch.6.L012060

Introduction. Multiple collaborations of pulsar timing array (PTA) have presented strong evidence for a signal exhibiting correlations consistent with a stochastic gravitational-wave background (GWB) [1–4]. The strain has been measured to be on the order of 10^{-15} at a pivot frequency of $1\ \mathrm{yr}^{-1}$. Though this GWB aligns with expectations from astrophysical sources, specifically inspiraling supper-massive black hole (SMBH) binaries [5], it is important to note that the current datasets do not rule out the possibility of cosmological origins or other exotic astrophysical sources, which have been explored in collaborative accompanying papers [6,7]. Notably, several cosmological models have demonstrated superior fits to the signal compared to the SMBH-binary interpretation. If these alternative models are confirmed in the future, they may provide compelling evidence for new physics.

Our focus lies on the cosmological interpretation of the signal, specifically the existence of scalar-induced gravitational waves (SIGWs) [8–13]. This possibility had been used for interpreting the NANOGrav 12.5-year dataset [14] in Refs. [15–24]. It was recently revisited by the PTA collaborations [6,7], but the statistics of primordial curvature perturbations was assumed to be Gaussian. However, it was demonstrated that primordial non-Gaussianity $f_{\rm NL}$ significantly contributes to the energy density of SIGWs [25–33]. This indicates noteworthy modifications to the energy-density spectrum, which is crucial for the data analysis of the recent PTA datasets, as studied by Ref. [34] during the preparation of our present paper. We will address the importance of $f_{\rm NL}$ to SIGWs through Bayesian analysis over the NANOGrav 15-year (NG15) data. On the other hand, it has been shown that primordial non-Gaussianity could generate initial inhomogeneities in SIGWs, leading to anisotropies characterized by the angular power spectrum [33]. Related studies can be found in Refs. [35–43]. Our analysis will also encompass a comprehensive examination of the angular power spectrum within the PTA band. Moreover, this spectrum is capable of breaking the degeneracies among model parameters, particularly leading to possible determination of $f_{\rm NL}$, and playing a crucial role in distinguishing between different sources of GWB. Therefore, by interpreting the signal as originating from SIGWs, we aim to study physical implications of PTA datasets for the nature of primordial curvature perturbations, including their power spectrum and angular power spectrum.

We will study implications of the aforementioned results for scenarios involving formation of primordial black holes (PBHs), which was accompanied by the production of SIGWs. Enhanced primordial curvature perturbations not only lead to formation of PBHs through gravitational collapse [44], but also produce GWB via nonlinear mode couplings. The study of SIGWs thus allows us to explore the PBH scenarios

*Corresponding author: zhaozc@cau.edu.cn

[45–52]. Related works analyzing observational datasets can be found in Refs. [6,7,20–22,48,53], and influence of primordial non-Gaussianity on the mass function of PBHs was also studied [24,54–67]. Taking $f_{\rm NL}$ into account, we will reinterpret the constraints on power spectrum as constraints on the mass range of PBHs.

SIGW energy-density fraction spectrum. Here, we show a brief but self-consistent summary of the main results of the energy-density fraction spectrum in a framework of SIGW theory.

For the homogeneous and isotropic component of a GWB, the energy-density fraction spectrum is defined as $\bar{\Omega}_{\rm gw}(\eta, q) = \bar{\rho}_{\rm gw}(\eta, q)/\rho_{\rm crit}(\eta)$ [68], where q represents the wavenumber, $\rho_{\rm crit}$ denotes the critical energy density of the universe at conformal time η, and the overbar signifies quantities at the background level. This definition implies that $\int \bar{\rho}_{\rm gw}(\eta, q)\mathrm{d}\ln q$ corresponds to the energy-density fraction of GWB [68]. The spectrum can be formally expressed as $\bar{\rho}_{\rm gw}(\eta, q) \sim \langle h_{ij,l} h_{ij,l}\rangle$, where $h_{ij}(\eta, \mathbf{q})$ represents the strain with wave vector $\mathbf{q}$, and the angle brackets denote an ensemble average. For subhorizon-scale SIGWs, we have $h_{ij} \sim \zeta^2$, leading to $\bar{\Omega}_{\rm gw}(\eta, \mathbf{q}) \sim \langle\zeta^4\rangle$ [8,9], where $\zeta(\mathbf{q})$ represents curvature perturbations in the early universe. In the case of primordial Gaussianity, semianalytic formulas for $\bar{\Omega}_{\rm gw}(\eta, \mathbf{q})$ were derived in Refs. [12,13], with earlier relevant works in Refs. [8,9]. However, in the presence of primordial non-Gaussianity $f_{\rm NL}$, there are not such semianalytic formulas. Recent literature provided relevant studies on this topic [25–33,69]. In this work, we adopt the conventions established in our previous study [33].

To quantify contributions of $f_{\rm NL}$ to the energy density of SIGWs, we express the primordial curvature perturbations ζ in terms of their Gaussian components ζ_g, i.e., [70]

$$\zeta(\mathbf{q}) = \zeta_g(\mathbf{q}) + \frac{3}{5} f_{\rm NL} \int \frac{\mathrm{d}^3\mathbf{k}}{(2\pi)^{3/2}} \zeta_g(\mathbf{k})\zeta_g(\mathbf{q}-\mathbf{k}). \quad (1)$$

Here, $f_{\rm NL}$ represents the nonlinear parameter that characterizes the local-type primordial non-Gaussianity. To simplify the subsequent analytic formulas, we introduce a new quantity as follows:

$$F_{\rm NL} = \tfrac{3}{5} f_{\rm NL}. \quad (2)$$

It is worth noting that perturbation theory requires the condition $A_S F_{\rm NL}^2 < 1$, where A_S will be defined later. We define the dimensionless power spectrum of ζ_g as

$$\langle\zeta_g(\mathbf{q})\zeta_g(\mathbf{q}')\rangle = \delta^{(3)}(\mathbf{q}+\mathbf{q}')\frac{2\pi^2}{q^3}\Delta_g^2(q). \quad (3)$$

We assume that $\Delta_g^2(q)$ follows a log-normal distribution with respect to $\ln q$ [21,31,71–73],

$$\Delta_g^2(q) = \frac{A_S}{\sqrt{2\pi\sigma^2}} \exp\left[-\frac{\ln^2(q/q_*)}{2\sigma^2}\right], \quad (4)$$

where A_S represents the spectral amplitude at the spectral peak wavenumber q_*, and σ denotes the standard deviation that characterizes the width of the spectrum. The wavenumber q is straightforwardly converted into the frequency ν, namely, $q = 2\pi\nu$.

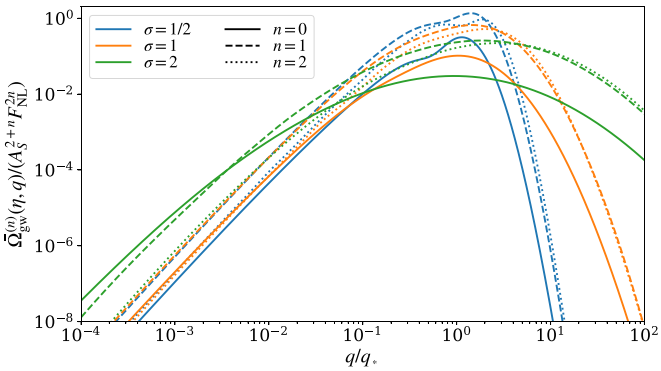

FIG. 1. Unscaled (or equivalently, $A_S = 1$ and $F_{\rm NL} = 1$) contributions to the energy-density fraction spectrum of SIGWs. We display $\sigma = 1/2, 1, 2$ and produce this figure by using the original data of Ref. [33].

Via detailed derivations based on Wick's theorem, we can decompose $\bar{\Omega}_{\rm gw} \sim \langle\zeta^4\rangle$ into three components depending on the power of $f_{\rm NL}$. The complete derivations have been simplified by employing a Feynman-like diagrammatic approach [25,28,30–33]. Here, we present the final results,

$$\bar{\Omega}_{\rm gw}(\eta, q) = \bar{\Omega}_{\rm gw}^{(0)}(\eta, q) + \bar{\Omega}_{\rm gw}^{(1)}(\eta, q) + \bar{\Omega}_{\rm gw}^{(2)}(\eta, q), \quad (5)$$

where we provide the analytic expressions for $\bar{\Omega}_{\rm gw}^{(n)}$, which are proportional to $A_S^2(A_S F_{\rm NL}^2)^n$ with $n = 0, 1, 2$, in the Appendix. They were evaluated using the `vegas` package [74], while their numerical results for $\sigma = 1/2, 1, 2$ are reproduced in Fig. 1. Specifically, $\bar{\Omega}_{\rm gw}^{(0)}$ corresponds to the energy-density fraction spectrum in the case of Gaussianity, while $\bar{\Omega}_{\rm gw}^{(1)}$ and $\bar{\Omega}_{\rm gw}^{(2)}$ fully describe the contributions of local-type primordial non-Gaussianity $f_{\rm NL}$.

The energy-density fraction spectrum of SIGWs at the present conformal time η_0 can be expressed as

$$\bar{\Omega}_{\rm gw,0}(\nu) = \Omega_{\rm rad,0}\left[\frac{g_{*,\rho}(T)}{g_{*,\rho}(T_{\rm eq})}\right]\left[\frac{g_{*,s}(T_{\rm eq})}{g_{*,s}(T)}\right]^{\frac{4}{3}} \bar{\Omega}_{\rm gw}(\eta, q). \quad (6)$$

In the above equation, $\Omega_{\rm rad,0}h^2 = 4.2 \times 10^{-5}$ represents the physical energy-density fraction of radiations in the present universe [75]. T and $T_{\rm eq}$ correspond to the cosmic temperatures at the emission time and the epoch of matter-radiation equality, respectively. ν can be related to T, $g_{*,\rho}(T)$, and $g_{*,s}(T)$ as follows [21]:

$$\frac{\nu}{\rm nHz} = 26.5\left(\frac{T}{\rm GeV}\right)\left[\frac{g_{*,\rho}(T)}{106.75}\right]^{\frac{1}{2}}\left[\frac{g_{*,s}(T)}{106.75}\right]^{-\frac{1}{3}}. \quad (7)$$

Here, $g_{*,\rho}$ and $g_{*,s}$ represent the effective relativistic degrees of freedom in the universe, which are tabulated functions of T as provided in Ref. [76]. To illustrate the interpretation of present PTA data in the framework of SIGWs, we depict $\bar{\Omega}_{\rm gw,0}(\nu)$ with respect to ν in Fig. 2, using three specific sets of model parameters.

Implications of PTA data for new physics. In this section, we investigate the potential constraints on the parameter space of the primordial power spectrum and PBHs using the NG15 data. While it is possible to obtain constraints from other PTA datasets using the same methodology, we do not consider

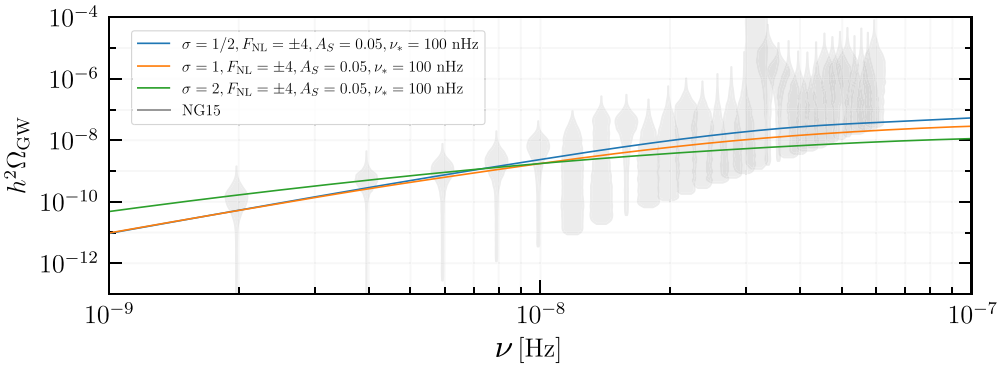

FIG. 2. Energy-density fraction spectra of SIGWs for different sets of independent parameters. The NG15 data are also shown for comparison.

them in this study, as they would not significantly alter the leading results of our present work.

Through performing a Bayesian analysis [7], we could gain valuable insights for the posteriors of four independent parameters, i.e., $F_{\rm NL}$, A_S, σ, and ν_*, for which the priors are set to be $F_{\rm NL} \in [-30, 30]$, $\log_{10} A_S \in [-3, 1]$, $\sigma \in [0, 5]$, and $\log_{10}(\nu_*/{\rm Hz}) \in [-9, -5]$. Here, we adopt the aforementioned condition of perturbativity, namely, $A_S F_{\rm NL}^2 < 1$. The inference results within 68% confidence intervals are given as

$$F_{\rm NL} = -0.00^{+2.45}_{-2.46}, \tag{8}$$

$$\log_{10} A_S = -0.97^{+0.65}_{-0.46}, \tag{9}$$

$$\sigma = 1.08^{+1.08}_{-0.83}, \tag{10}$$

$$\log_{10}(\nu_*/{\rm Hz}) = -6.99^{+0.93}_{-0.45}. \tag{11}$$

We can also recast Eq. (8) into constraints on $f_{\rm NL}$, i.e.,

$$f_{\rm NL} = -0.0 \pm 4.1. \tag{12}$$

Figure 3 shows two-dimensional contours in $\log_{10} A_S - F_{\rm NL}$ plane at 68% (dark blue regions) and 95% (light blue regions) confidence levels. There is a full degeneracy in the sign of

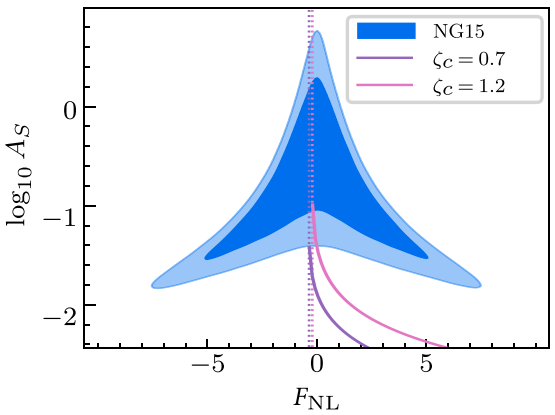

FIG. 3. Two-dimensional contours (blue shaded) in the $\log_{10} A_S - F_{\rm NL}$ plane inferred from the NG15 data. Dotted lines denote $F_{\rm NL} = -(4\zeta_c)^{-1}$ while solid curves stand for models, which expect $f_{\rm pbh} = 1$ for $m_{\rm pbh} = 10^{-2} M_\odot$, in the cases of $\zeta_c = 0.7$ (purple) and $\zeta_c = 1.2$ (rose), respectively.

primordial non-Gaussianity $f_{\rm NL}$, as the energy-density fraction spectrum is dependent of only the absolute value of $F_{\rm NL}$, as demonstrated in Fig. 1. The above results indicate that the PTA observations have already emerged as a powerful tool for probing physics of the early universe. We can further recast the constraints on the primordial curvature power spectrum into constraints on the nature of PBHs, which is characterized by their mass function. Due to significant uncertainties in the formation scenarios of PBHs (as discussed in reviews such as Ref. [43]), we adopt a simplified scenario [62] to illustrate the importance of $f_{\rm NL}$. Though it is an approximation, our results would be consistent with those from numerical relativistic simulations [77]. The initial mass function of PBHs is described by

$$\beta = \int_{\zeta > \zeta_c} P(\zeta) d\zeta = \int_{\zeta(\zeta_g) > \zeta_c} \frac{1}{\sqrt{2\pi}\sigma_g} \exp\left(-\frac{\zeta_g^2}{2\sigma_g^2}\right) d\zeta_g, \tag{13}$$

where $P(\zeta)$ represents the probability distribution function (PDF) of primordial curvature perturbations, σ_g is the standard variance of the Gaussian component ζ_g in the PDF, and ζ_c stands for the critical fluctuation. We further find $\sigma_g^2 = \langle \zeta_g^2 \rangle = \int \Delta_g^2(q) d\ln q = A_S$ by considering the power spectrum defined in Eq. (4). Additionally, it is known that ζ_c is of order $\mathcal{O}(1)$, with specific values of 0.7 and 1.2, as suggested by Ref. [78].

To evaluate Eq. (13), we divide $F_{\rm NL}$ into two regimes, i.e., $F_{\rm NL} > 0$ and $F_{\rm NL} < 0$. In the case of $F_{\rm NL} > 0$, we solve the equation $\zeta(\zeta_g) = \zeta_c$, yielding a relation

$$\zeta_{g\pm} = \frac{-1 \pm \sqrt{1 + 4F_{\rm NL}\zeta_c}}{2F_{\rm NL}}. \tag{14}$$

By substituting it into Eq. (13), we gain

$$\begin{aligned} \beta &= \left(\int_{-\infty}^{\zeta_{g-}} + \int_{\zeta_{g+}}^{+\infty}\right) P(\zeta_g) d\zeta_g \\ &= \frac{1}{2}{\rm erfc}\left(\frac{\zeta_{g+}}{\sqrt{2A_S}}\right) + \frac{1}{2}{\rm erfc}\left(-\frac{\zeta_{g-}}{\sqrt{2A_S}}\right), \end{aligned} \tag{15}$$

where erfc(x) is the complementary error function. Similarly, in the case of $-(4\zeta_c)^{-1} < F_{\rm NL} < 0$, we gain

$$\beta = \int_{\zeta_{g+}}^{\zeta_{g-}} P(\zeta_g) d\zeta_g = \frac{1}{2}\mathrm{erfc}\left(\frac{\zeta_{g+}}{\sqrt{2A_S}}\right) - \frac{1}{2}\mathrm{erfc}\left(\frac{\zeta_{g-}}{\sqrt{2A_S}}\right). \tag{16}$$

In contrast, in the case of $F_{\rm NL} < -(4\zeta_c)^{-1}$, no PBHs were formed in the early universe, since the curvature perturbations are expected to never exceed the critical fluctuation. As a viable candidate for cold dark matter, the abundance of PBHs is determined as [79]

$$f_{\rm pbh} \simeq 2.5 \times 10^8 \beta \left[\frac{g_{*,\rho}(T_{\rm f})}{10.75}\right]^{-\frac{1}{4}} \left[\frac{m_{\rm pbh}}{M_\odot}\right]^{-\frac{1}{2}}, \tag{17}$$

where $m_{\rm pbh}$ represents the mass of PBHs, and $T_{\rm f}$ denotes cosmic temperature at the formation occasion. Roughly speaking, $m_{\rm pbh}$ can be related to the horizon mass m_H and then the peak frequency ν_*, namely, [17]

$$\frac{m_{\rm pbh}}{M_\odot} \simeq \frac{m_H}{0.31 M_\odot} \simeq \left(\frac{\nu_*}{5.0\mathrm{nHz}}\right)^{-2}. \tag{18}$$

Based on Eq. (11), we could infer that the mass range of PBHs is the order of $\mathcal{O}(10^{-5}-10^{-2})M_\odot$. However, the inferred abundance of PBHs exceeds unity in the case of a sizable positive $F_{\rm NL}$, indicating an overproduction of PBHs. This is because the inferred value of A_S is typically one order of magnitude larger than the value of A_S that leads to $f_{\rm pbh} = 1$. To illustrate this result more clearly, we include in Fig. 3 two solid curves corresponding to $m_{\rm pbh} = 10^{-2} M_\odot$ and $f_{\rm pbh} = 1$ in the cases of $\zeta_c = 0.7$ (purple curve) and $\zeta_c = 1.2$ (rose curve), respectively. For comparison, we mark the critical value $F_{\rm NL} = -(4\zeta_c)^{-1}$ with dotted lines. Therefore, we find that a negative $F_{\rm NL}$ is capable of alleviating the overproduction of PBHs, especially when considering a sizable negative $F_{\rm NL}$, namely, $F_{\rm NL} < -(4\zeta_c)^{-1}$, which prevents the formation of any PBHs. However, due to large uncertainties in model buildings, it remains challenging to exclude the PBH scenario through analyzing the present PTA data.

In summary, it is crucial to measure the primordial non-Gaussianity or at least determine the sign of $F_{\rm NL}$ in order to assess the viability of the PBH scenario. However, it is impossible to determine the sign of $F_{\rm NL}$ through measurements of the energy-density fraction spectrum of SIGWs, due to the sign degeneracy. In the next section, we will propose that the inhomogeneous and anisotropic component of SIGWs has the potential to break the sign degeneracy, as well as other degeneracies in model parameters, opening up new possibilities for making judgments about the PBH scenario in the future.

SIGW angular power spectrum. Here, we investigate the inhomogeneities and anisotropies in SIGWs via deriving the angular power spectrum in the PTA band, following the research approach established in our existing paper [33].

The inhomogeneities in SIGWs arise from the long-wavelength modulations of the energy density generated by short-wavelength modes. As discussed above, SIGWs originate from extremely high redshifts, corresponding to very small horizons. However, due to limitations in the angular resolution of detectors, the signal along a line-of-sight represents an ensemble average of the energy densities over a sizable number of such horizons. Consequently, any two signals would appear identical. Nevertheless, the energy density of SIGWs produced by short-wavelength modes can be spatially redistributed by long-wavelength modes if there are couplings between the two. The local-type primordial non-Gaussianity could contribute to such couplings.

Similar to the temperature fluctuations of relic photons [80], the initial inhomogeneities in SIGWs at a spatial location $\mathbf{x}$ can be characterized by the density contrast, which is denoted as $\delta_{\rm gw}(\eta, \mathbf{x}, \mathbf{q})$, given by

$$\delta_{\rm gw}(\eta, \mathbf{x}, \mathbf{q}) = 4\pi \frac{\omega_{\rm gw}(\eta, \mathbf{x}, \mathbf{q})}{\bar{\Omega}_{\rm gw}(\eta, q)} - 1, \tag{19}$$

where the energy-density full spectrum $\omega_{\rm gw}(\eta, \mathbf{x}, \mathbf{q})$ is defined in terms of the energy density, namely, $\rho_{\rm gw}(\eta, \mathbf{x}) = \rho_{\rm crit}(\eta) \int \mathrm{d}^3\mathbf{q}, \omega_{\rm gw}(\eta, \mathbf{x}, \mathbf{q})/q^3$. We specifically get $\omega_{\rm gw} \sim \langle \zeta^4 \rangle_{\mathbf{x}}$, where the subscript $_{\mathbf{x}}$ denotes an ensemble average within the horizon enclosing $\mathbf{x}$ [33,35]. We decompose ζ_g into modes of short wavelength ζ_{gS} and long wavelength ζ_{gL}, namely, $\zeta_g = \zeta_{gS} + \zeta_{gL}$ [81]. At linear order in ζ_{gL}, we get $\delta_{\rm gw} \sim \zeta_{gL} \langle \zeta_{gS} \zeta_S^3 \rangle_{\mathbf{x}}$, where ζ_S represents the part of ζ composed solely of ζ_{gS}. Terms of higher orders in ζ_{gL} are negligible due to smallness of the power spectrum $\Delta_L^2 \sim 10^{-9}$ [75]. Using Feynman-like rules and diagrams, we get an expression for $\delta_{\rm gw}(\eta, \mathbf{x}, \mathbf{q})$, i.e., [33]

$$\delta_{\rm gw}(\eta, \mathbf{x}, \mathbf{q}) = F_{\rm NL} \frac{\Omega_{\rm ng}(\eta, q)}{\bar{\Omega}_{\rm gw}(\eta, q)} \int \frac{d^3\mathbf{k}}{(2\pi)^{3/2}} e^{i\mathbf{k}\cdot\mathbf{x}} \zeta_{gL}(\mathbf{k}), \tag{20}$$

where we introduce a quantity of the form

$$\Omega_{\rm ng}(\eta, q) = 2^3 \bar{\Omega}_{\rm gw}^{(0)}(\eta, q) + 2^2 \bar{\Omega}_{\rm gw}^{(1)}(\eta, q). \tag{21}$$

The present density contrast, denoted as $\delta_{\rm gw,0}(\mathbf{q})$, can be estimated analytically using the line-of-sight approach [82–84]. It is contributed by both the initial inhomogeneities and propagation effects, given by [35]

$$\delta_{\rm gw,0}(\mathbf{q}) = \delta_{\rm gw}(\eta, \mathbf{x}, \mathbf{q}) + [4 - n_{\rm gw,0}(\nu)]\Phi(\eta, \mathbf{x}). \tag{22}$$

Here, $n_{\rm gw,0}(\mathbf{q})$ denotes the index of the present energy-density fraction spectrum in Eq. (6), given by

$$n_{\rm gw,0}(\nu) = \frac{\partial \ln \bar{\Omega}_{\rm gw,0}(\nu)}{\partial \ln \nu} \simeq \left.\frac{\partial \ln \bar{\Omega}_{\rm gw}(\eta, q)}{\partial \ln q}\right|_{q=2\pi\nu}. \tag{23}$$

For the propagation effects, we consider only the Sachs-Wolfe (SW) effect [85], which is characterized by the Bardeen's potential on large scales

$$\Phi(\eta, \mathbf{x}) = \frac{3}{5} \int \frac{d^3\mathbf{k}}{(2\pi)^{3/2}} e^{i\mathbf{k}\cdot\mathbf{x}} \zeta_{gL}(\mathbf{k}). \tag{24}$$

We assume the statistical homogeneity and isotropy for the density contrasts on large scales, similar to the study of cosmic microwave background (CMB) [86].

The anisotropies today can be mapped from the aforementioned inhomogeneities. The reduced angular power spectrum is useful to characterize the statistics of these anisotropies. It is defined as the two-point correlator of the present density contrast, namely,

$$\langle \delta_{\rm gw,0,\ell m}(2\pi\nu) \delta^*_{\rm gw,0,\ell' m'}(2\pi\nu) \rangle = \delta_{\ell\ell'} \delta_{mm'} \widetilde{C}_\ell(\nu), \tag{25}$$

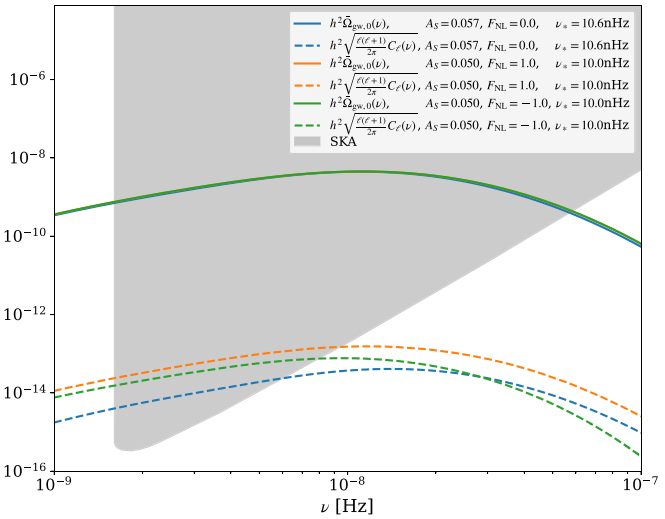

FIG. 4. Physical energy-density fraction spectra of SIGWs, $h^2\Omega_{\rm gw,0}(\nu)$ (solid), and the variance of SIGW density contrasts, $h^2[\ell(\ell+1)C_\ell(\nu)/(2\pi)]^{1/2}$ (dashed). For comparison, we show the sensitivity region of SKA [87] (gray shaded).

where $\delta_{\rm gw,0}(\mathbf{q})$ has been expanded in terms of spherical harmonics, i.e.,

$$\delta_{\rm gw,0}(\mathbf{q}) = \sum_{\ell m} \delta_{{\rm gw,0},\ell m}(q) Y_{\ell m}(\mathbf{n}). \tag{26}$$

We roughly get $\widetilde{C}_\ell \sim \delta^2_{\rm gw,0} \propto \langle \zeta_{gL}\zeta_{gL}\rangle \sim \Delta^2_L$. Detailed analysis using the Feynman-like rules and diagrams was conducted in Ref. [33]. Under the assumption of low-ℓ multipoles, we summarize the main results as

$$\widetilde{C}_\ell = \frac{18\pi\Delta^2_L}{25\ell(\ell+1)}\left\{f_{\rm NL}\frac{\Omega_{\rm ng}}{\bar{\Omega}_{\rm gw}} + [4 - n_{\rm gw,0}]\right\}^2, \tag{27}$$

which is recast into the angular power spectrum

$$C_\ell(\nu) = \left[\frac{\bar{\Omega}_{\rm gw,0}(\nu)}{4\pi}\right]^2 \tilde{C}_\ell(\nu). \tag{28}$$

Analogous to CMB, for which the root-mean-square (rms) temperature fluctuations is $[\ell(\ell+1)C^{\rm CMB}_\ell/(2\pi)]^{1/2}$, the rms density contrast for SIGWs is $[\ell(\ell+1)C_\ell(\nu)/(2\pi)]^{1/2}$, which represents the variance of the energy-density fluctuations. Note that the rms density contrast is constant with respect to ℓ, but depends on frequency bands.

In Fig. 4, we present the rms density contrast as a function of gravitational-wave frequency. We also include the energy-density fraction spectrum for comparison. We find that $\sqrt{\widetilde{C}_\ell}$ is roughly the order of 10^{-4}, depending on specific model parameters. It is worth noting that the angular power spectrum can break degeneracies among these parameters. For instance, based on Fig. 4, we observe a coincidence in the energy-density fraction spectra for three different parameter sets. However, the angular power spectrum breaks this coincidence, particularly in the case of the sign degeneracy of $f_{\rm NL}$. This result suggests that measurements of the anisotropies in SIGWs have the potential to determine the primordial non-Gaussianity [33]. Recently, an upper limit of $\tilde{C}_\ell < 20\%$ was inferred from the NG15 data [88]. However, this limit is not precise enough to test the theoretical predictions of our present work. In contrast, based on Fig. 4, we anticipate that the Square Kilometre Array (SKA) program [87] will offer sufficient precision to measure the non-Gaussianity $f_{\rm NL}$.

Conclusions. In this study, we examined the implications of recent PTA datasets for understanding the nature of primordial curvature perturbations and primordial black holes (PBHs). Specifically, we investigated the influence of primordial non-Gaussianity $f_{\rm NL}$ on the inference of model parameters, and vice versa, by analyzing the recent NG15 data. In particular, at 68% confidence level, we inferred $|f_{\rm NL}| < 4.1$, which is competitive with the constraints from measurements of CMB. Even when considering the non-Gaussianity $f_{\rm NL}$, we found that the PBH scenario is in tension with the NG15 data, except when a sizable negative $f_{\rm NL}$ is considered, which can significantly suppress the abundance of PBHs. Our results indicated that the PTA observations have already emerged as a powerful tool for probing physics of the early universe and dark matter. Moreover, we proposed that the anisotropies of SIGWs serve as a powerful probe of the primordial non-Gaussianity in the PTA band. For the first time, we conducted the complete analysis of the angular power spectrum in this frequency band and found that it can effectively break potential degeneracies among the model parameters, particularly the sign degeneracy of $f_{\rm NL}$. Additionally, we explored the detectability of the anisotropies in SIGWs in the era of the SKA project.

Acknowledgments. S.W. and J.P.L. are supported by the National Natural Science Foundation of China (Grant No. 12175243), the National Key R&D Program of China No. 2023YFC2206403, the Science Research Grants from the China Manned Space Project with No. CMS-CSST-2021-B01, and the Key Research Program of the Chinese Academy of Sciences (Grant No. XDPB15). Z.C.Z. is supported by the National Key Research and Development Program of China Grant No. 2021YFC2203001 and the National Natural Science Foundation of China (Grant No. 12005016). Q.H.Z. is supported by the National Nature Science Foundation of China (Grant No. 12305073). This work is supported by the High-performance Computing Platform of China Agricultural University.

Appendix:

Formulae for evaluating the SIGW energy density. After a comprehensive derivation following the methodology presented in Refs. [31–33], we can precisely express the three terms in Eq. (5) as

$$\bar{\Omega}^{(0)}_{\rm gw}(\eta, q) = \frac{1}{3}\int_0^\infty dt_1 \int_{-1}^1 ds_1 \overline{I^2(u_1, v_1, x\to\infty)}\frac{1}{(u_1 v_1)^2}\Delta^2_g(v_1 q)\Delta^2_g(u_1 q), \tag{A1}$$

$$\bar{\Omega}_{\rm gw}^{(1)}(\eta,q)=\frac{F_{\rm NL}^2}{3\pi}\prod_{i=1}^{2}\left[\int_0^\infty dt_i\int_{-1}^{1}ds_i\,v_iu_i\right]\left\{\frac{\pi\overline{J^2(u_1,v_1,x\to\infty)}}{(u_1v_1u_2v_2)^3}\Delta_g^2(v_1v_2q)\Delta_g^2(u_1q)\Delta_g^2(v_1u_2q)\right.$$
$$\left.+\int_0^{2\pi}d\varphi_{12}\,\cos 2\varphi_{12}\overline{J(u_1,v_1,x\to\infty)J(u_2,v_2,x\to\infty)}\frac{\Delta_g^2(v_2q)}{v_2^3}\frac{\Delta_g^2(w_{12}q)}{w_{12}^3}\left[\frac{\Delta_g^2(u_2q)}{u_2^3}+\frac{\Delta_g^2(u_1q)}{u_1^3}\right]\right\},\tag{A2}$$

$$\bar{\Omega}_{\rm gw}^{(2)}(\eta,q)=\frac{F_{\rm NL}^4}{24\pi^2}\prod_{i=1}^{3}\left[\int_0^\infty dt_i\int_{-1}^{1}ds_i\,v_iu_i\right]\left\{\frac{2\pi^2\overline{J^2(u_1,v_1,x\to\infty)}}{(u_1v_1u_2v_2u_3v_3)^3}\Delta_g^2(v_1v_2q)\Delta_g^2(v_1u_2q)\Delta_g^2(u_1v_3q)\Delta_g^2(u_1u_3q)\right.$$
$$+\int_0^{2\pi}d\varphi_{12}d\varphi_{23}\,\cos 2\varphi_{12}\overline{J(u_1,v_1,x\to\infty)J(u_2,v_2,x\to\infty)}$$
$$\left.\times\frac{\Delta_g^2(u_3q)}{u_3^3}\frac{\Delta_g^2(w_{13}q)}{w_{13}^3}\left[\frac{\Delta_g^2(v_3q)}{v_3^3}\frac{\Delta_g^2(w_{23}q)}{w_{23}^3}+\frac{\Delta_g^2(w_{23}q)}{w_{23}^3}\frac{\Delta_g^2(w_{123}q)}{w_{123}^3}\right]\right\},\tag{A3}$$

where we define $x=q\eta$, $s_i=u_i-v_i$, $t_i=u_i+v_i-1$, and

$$y_{ij}=\frac{\cos\varphi_{ij}}{4}\sqrt{t_i(t_i+2)\left(1-s_i^2\right)t_j(t_j+2)\left(1-s_j^2\right)}+\frac{1}{4}[1-s_i(t_i+1)][1-s_j(t_j+1)],\tag{A4a}$$

$$w_{ij}=\sqrt{v_i^2+v_j^2-y_{ij}},\tag{A4b}$$

$$w_{123}=\sqrt{v_1^2+v_2^2+v_3^2+y_{12}-y_{13}-y_{23}}.\tag{A4c}$$

The calculation for the average of the squared oscillation $J(u,v,x\to\infty)$ has been provided in Ref. [33], as well as in earlier studies referenced in Refs. [12,13,30,31], i.e.,

$$\overline{J(u_i,v_i,x\to\infty)J(u_j,v_j,x\to\infty)}=\frac{9\left(1-s_i^2\right)\left(1-s_j^2\right)t_i(t_i+2)t_j(t_j+2)\left(s_i^2+t_i^2+2t_i-5\right)\left(s_j^2+t_j^2+2t_j-5\right)}{8(-s_i+t_i+1)^3(s_i+t_i+1)^3(-s_j+t_j+1)^3(s_j+t_j+1)^3}$$
$$\times\left\{\left[\left(s_i^2+t_i^2+2t_i-5\right)\ln\left(\left|\frac{t_i^2+2t_i-2}{s_i^2-3}\right|\right)+2(s_i-t_i-1)(s_i+t_i+1)\right]\right.$$
$$\times\left[\left(s_j^2+t_j^2+2t_j-5\right)\ln\left(\left|\frac{t_j^2+2t_j-2}{s_j^2-3}\right|\right)+2(s_j-t_j-1)(s_j+t_j+1)\right]$$
$$\left.+\pi^2\Theta(t_i-\sqrt{3}+1)\Theta(t_j-\sqrt{3}+1)\left(s_i^2+t_i^2+2t_i-5\right)\left(s_j^2+t_j^2+2t_j-5\right)\right\}.\tag{A5}$$

The equations presented in this Appendix can be utilized to numerically calculate the energy density of SIGWs in a self-consistent manner.

[1] H. Xu *et al.*, Searching for the nano-Hertz stochastic gravitational wave background with the chinese pulsar timing array data release I, Res. Astron. Astrophys. **23**, 075024 (2023).

[2] J. Antoniadis *et al.*, The second data release from the European Pulsar Timing Array III. Search for gravitational wave signals, Astron. Astrophys. **678**, A50 (2023).

[3] G. Agazie *et al.*, The NANOGrav 15-year data set: Evidence for a gravitational-wave background, Astrophys. J. Lett. **951**, L8 (2023).

[4] D. J. Reardon *et al.*, Search for an isotropic gravitational-wave background with the Parkes Pulsar Timing Array, Astrophys. J. Lett. **951**, L6 (2023).

[5] G. Agazie *et al.*, The NANOGrav 15-year data set: Constraints on supermassive black hole binaries from the gravitational wave background, Astrophys. J. Lett. **952**, L37 (2023).

[6] J. Antoniadis *et al.*, The second data release from the European Pulsar Timing Array: V. Implications for massive black holes, dark matter and the early Universe, arXiv:2306.16227.

[7] A. Afzal *et al.*, The NANOGrav 15-year data set: Search for signals from new physics, Astrophys. J. Lett. **951**, L11 (2023).

[8] K. N. Ananda, C. Clarkson, and D. Wands, The cosmological gravitational wave background from primordial density perturbations, Phys. Rev. D **75**, 123518 (2007).

[9] D. Baumann, P. J. Steinhardt, K. Takahashi, and K. Ichiki, Gravitational wave spectrum induced by primordial scalar perturbations, Phys. Rev. D **76**, 084019 (2007).

[10] S. Mollerach, D. Harari, and S. Matarrese, CMB polarization from secondary vector and tensor modes, Phys. Rev. D **69**, 063002 (2004).

[11] H. Assadullahi and D. Wands, Constraints on primordial density perturbations from induced gravitational waves, Phys. Rev. D **81**, 023527 (2010).

[12] J. R. Espinosa, D. Racco, and A. Riotto, A cosmological signature of the sm higgs instability: Gravitational waves, J. Cosmol. Astropart. Phys. 09 (2018) 012.

[13] K. Kohri and T. Terada, Semianalytic calculation of gravitational wave spectrum nonlinearly induced from primordial curvature perturbations, Phys. Rev. D **97**, 123532 (2018).

[14] Z. Arzoumanian *et al.*, The NANOGrav 12.5 yr data set: Search for an isotropic stochastic gravitational-wave background, Astrophys. J. Lett. **905**, L34 (2020).

[15] V. De Luca, G. Franciolini, and A. Riotto, NANOGrav data hints at primordial black holes as dark matter, Phys. Rev. Lett. **126**, 041303 (2021).

[16] V. Vaskonen and H. Veermäe, Did NANOGrav see a signal from primordial black hole formation? Phys. Rev. Lett. **126**, 051303 (2021).

[17] K. Kohri and T. Terada, Solar-mass primordial black holes explain NANOGrav hint of gravitational waves, Phys. Lett. B **813**, 136040 (2021).

[18] G. Domènech and S. Pi, NANOGrav hints on planet-mass primordial black holes, Sci. China Phys. Mech. Astron. **65**, 230411 (2022).

[19] V. Atal, A. Sanglas, and N. Triantafyllou, NANOGrav signal as mergers of stupendously large primordial black holes, J. Cosmol. Astropart. Phys. 06 (2021) 022.

[20] Z. Yi and Q. Fei, Constraints on primordial curvature spectrum from primordial black holes and scalar-induced gravitational waves, Eur. Phys. J. C **83**, 82 (2023).

[21] Z.-C. Zhao and S. Wang, Bayesian implications for the primordial black holes from NANOGrav's pulsar-timing data using the scalar-induced gravitational waves, Universe **9**, 157 (2023).

[22] V. Dandoy, V. Domcke, and F. Rompineve, Search for scalar induced gravitational waves in the International Pulsar Timing Array Data Release 2 and NANOgrav 12.5 years dataset, SciPost Phys. Core **6**, 060 (2023).

[23] R.-G. Cai, C. Chen, and C. Fu, Primordial black holes and stochastic gravitational wave background from inflation with a noncanonical spectator field, Phys. Rev. D **104**, 083537 (2021).

[24] K. Inomata, M. Kawasaki, K. Mukaida, and T. T. Yanagida, NANOGrav results and LIGO-Virgo primordial black holes in axionlike curvaton models, Phys. Rev. Lett. **126**, 131301 (2021).

[25] J. García-Bellido, M. Peloso, and C. Unal, Gravitational wave signatures of inflationary models from primordial black hole dark matter, J. Cosmol. Astropart. Phys. 09 (2017) 013.

[26] G. Domènech and M. Sasaki, Hamiltonian approach to second order gauge invariant cosmological perturbations, Phys. Rev. D **97**, 023521 (2018).

[27] Rong-gen Cai, S. Pi, and M. Sasaki, Gravitational waves induced by non-gaussian scalar perturbations, Phys. Rev. Lett. **122**, 201101 (2019).

[28] C. Ünal, Imprints of primordial non-Gaussianity on gravitational wave spectrum, Phys. Rev. D **99**, 041301(R) (2019).

[29] C. Yuan and Q.-G. Huang, Gravitational waves induced by the local-type non-Gaussian curvature perturbations, Phys. Lett. B **821**, 136606 (2021).

[30] V. Atal and G. Domènech, Probing non-Gaussianities with the high frequency tail of induced gravitational waves, J. Cosmol. Astropart. Phys. 06 (2021) 001.

[31] P. Adshead, K. D. Lozanov, and Z. J. Weiner, Non-Gaussianity and the induced gravitational wave background, J. Cosmol. Astropart. Phys. 10 (2021) 080.

[32] H. V. Ragavendra, Accounting for scalar non-Gaussianity in secondary gravitational waves, Phys. Rev. D **105**, 063533 (2022).

[33] J.-P. Li, S. Wang, Z.-C. Zhao, and K. Kohri, Primordial non-Gaussianity f_{NL} and anisotropies in scalar-induced gravitational waves, J. Cosmol. Astropart. Phys. **10** (2023) 056.

[34] G. Franciolini, A. J. Iovino, V. Vaskonen, and H. Veermae, The recent gravitational wave observation by pulsar timing arrays and primordial black holes: the importance of non-gaussianities, Phys. Rev. Lett. **131**, 201401 (2023).

[35] N. Bartolo, D. Bertacca, V. De Luca, G. Franciolini, S. Matarrese, M. Peloso, A. Ricciardone, A. Riotto, and G. Tasinato, Gravitational wave anisotropies from primordial black holes, J. Cosmol. Astropart. Phys. 02 (2020) 028.

[36] L. Valbusa Dall'Armi, A. Ricciardone, N. Bartolo, D. Bertacca, and S. Matarrese, Imprint of relativistic particles on the anisotropies of the stochastic gravitational-wave background, Phys. Rev. D **103**, 023522 (2021).

[37] E. Dimastrogiovanni, M. Fasiello, A. Malhotra, P. D. Meerburg, and G. Orlando, Testing the early universe with anisotropies of the gravitational wave background, J. Cosmol. Astropart. Phys. 02 (2022) 040.

[38] F. Schulze, L. V. Dall'Armi, J. Lesgourgues, A. Ricciardone, N. Bartolo, D. Bertacca, C. Fidler, and S. Matarrese, GW_CLASS: Cosmological gravitational wave background in the cosmic linear anisotropy solving system, J. Cosmol. Astropart. Phys. **10** (2023) 025.

[39] N. Bartolo *et al.*, Probing anisotropies of the stochastic gravitational wave background with LISA, J. Cosmol. Astropart. Phys. 11 (2022) 009.

[40] P. Auclair *et al.*, Cosmology with the laser interferometer space antenna, Living Rev. Rel. **26**, 5 (2023).

[41] C. Ünal, E. D. Kovetz, and S. P. Patil, Multimessenger probes of inflationary fluctuations and primordial black holes, Phys. Rev. D **103**, 063519 (2021).

[42] A. Malhotra, E. Dimastrogiovanni, M. Fasiello, and M. Shiraishi, Cross-correlations as a diagnostic tool for primordial gravitational waves, J. Cosmol. Astropart. Phys. 03 (2021) 088.

[43] B. Carr, K. Kohri, Y. Sendouda, and J. Yokoyama, Constraints on primordial black holes, Rep. Prog. Phys. **84**, 116902 (2021).

[44] S. Hawking, Gravitationally collapsed objects of very low mass, Mon. Not. Roy. Astron. Soc. **152**, 75 (1971).

[45] E. Bugaev and P. Klimai, Induced gravitational wave background and primordial black holes, Phys. Rev. D **81**, 023517 (2010).

[46] R. Saito and J. Yokoyama, Gravitational-wave constraints on the abundance of primordial black holes, Prog. Theor. Phys. **123**, 867 (2010); **126**, 351(E) (2011).

[47] S. Wang, T. Terada, and K. Kohri, Prospective constraints on the primordial black hole abundance from the stochastic gravitational-wave backgrounds produced by coalescing events and curvature perturbations, Phys. Rev. D **99**, 103531 (2019); **101**, 069901(E) (2020).

[48] S. J. Kapadia, K. L. Pandey, T. Suyama, S. Kandhasamy, and P. Ajith, Search for the stochastic gravitational-wave background induced by primordial curvature perturbations in LIGO's second observing run, Astrophys. J. Lett. **910**, L4 (2021).

[49] Z.-C. Chen, C. Yuan, and Q.-G. Huang, Pulsar timing array constraints on primordial black holes with NANOGrav 11-year data set, Phys. Rev. Lett. **124**, 251101 (2020).

[50] T. Papanikolaou, Gravitational waves induced from primordial black hole fluctuations: the effect of an extended mass function, J. Cosmol. Astropart. Phys. 10 (2022) 089.

[51] T. Papanikolaou, V. Vennin, and D. Langlois, Gravitational waves from a universe filled with primordial black holes, J. Cosmol. Astropart. Phys. 03 (2021) 053.

[52] E. Madge, E. Morgante, C. Puchades Ibáñez, N. Ramberg, and S. Schenk, Primordial gravitational waves in the nano-Hertz regime and PTA data – towards solving the GW inverse problem, J. High Energ. Phys. **10** (2023) 171.

[53] A. Romero-Rodríguez, M. Martinez, O. Pujolàs, M. Sakellariadou, and V. Vaskonen, Search for a scalar induced stochastic gravitational wave background in the third LIGO-Virgo observing run, Phys. Rev. Lett. **128**, 051301 (2022).

[54] J. S. Bullock and J. R. Primack, Non-Gaussian fluctuations and primordial black holes from inflation, Phys. Rev. D **55**, 7423 (1997).

[55] C. T. Byrnes, E. J. Copeland, and A. M. Green, Primordial black holes as a tool for constraining non-Gaussianity, Phys. Rev. D **86**, 043512 (2012).

[56] S. Young and C. T. Byrnes, Primordial black holes in non-Gaussian regimes, J. Cosmol. Astropart. Phys. 08 (2013) 052.

[57] G. Franciolini, A. Kehagias, S. Matarrese, and A. Riotto, Primordial black holes from inflation and non-Gaussianity, J. Cosmol. Astropart. Phys. 03 (2018) 016.

[58] S. Passaglia, W. Hu, and H. Motohashi, Primordial black holes and local non-Gaussianity in canonical inflation, Phys. Rev. D **99**, 043536 (2019).

[59] V. Atal and C. Germani, The role of non-gaussianities in primordial black hole formation, Phys. Dark Univ. **24**, 100275 (2019).

[60] V. Atal, J. Garriga, and A. Marcos-Caballero, Primordial black hole formation with non-Gaussian curvature perturbations, J. Cosmol. Astropart. Phys. 09 (2019) 073.

[61] M. Taoso and A. Urbano, Non-gaussianities for primordial black hole formation, J. Cosmol. Astropart. Phys. 08 (2021) 016.

[62] D.-S. Meng, C. Yuan, and Qing-guo Huang, One-loop correction to the enhanced curvature perturbation with local-type non-Gaussianity for the formation of primordial black holes, Phys. Rev. D **106**, 063508 (2022).

[63] C. Chen, A. Ghoshal, Z. Lalak, Y. Luo, and A. Naskar, Growth of curvature perturbations for PBH formation in non-minimal curvaton scenario revisited, J. Cosmol. Astropart. Phys. **08** (2023) 041.

[64] R. Kawaguchi, T. Fujita, and M. Sasaki, Highly asymmetric probability distribution from a finite-width upward step during inflation, J. Cosmol. Astropart. Phys. **11** (2023) 021.

[65] C. Fu, P. Wu, and H. Yu, Primordial black holes and oscillating gravitational waves in slow-roll and slow-climb inflation with an intermediate noninflationary phase, Phys. Rev. D **102**, 043527 (2020).

[66] S. Young, C. T. Byrnes, and M. Sasaki, Calculating the mass fraction of primordial black holes, J. Cosmol. Astropart. Phys. 07 (2014) 045.

[67] S. Choudhury, A. Karde, S. Panda, and M. Sami, Primordial non-Gaussianity from ultra slow-roll Galileon inflation, J. Cosmol. Astropart. Phys. **01** (2024) 012.

[68] M. Maggiore, Gravitational wave experiments and early universe cosmology, Phys. Rep. **331**, 283 (2000).

[69] S. Garcia-Saenz, L. Pinol, S. Renaux-Petel, and D. Werth, No-go theorem for scalar-trispectrum-induced gravitational waves, J. Cosmol. Astropart. Phys. 03 (2023) 057.

[70] E. Komatsu and D. N. Spergel, Acoustic signatures in the primary microwave background bispectrum, Phys. Rev. D **63**, 063002 (2001).

[71] S. Pi and M. Sasaki, Gravitational waves induced by scalar perturbations with a lognormal peak, J. Cosmol. Astropart. Phys. 09 (2020) 037.

[72] E. Dimastrogiovanni, M. Fasiello, A. Malhotra, and G. Tasinato, Enhancing gravitational wave anisotropies with peaked scalar sources, J. Cosmol. Astropart. Phys. 01 (2023) 018.

[73] J. Cang, Y.-Z. Ma, and Y. Gao, Implications for primordial black holes from cosmological constraints on scalar-induced gravitational waves, Astrophys. J. **949**, 64 (2023).

[74] G. P. Lepage, Adaptive multidimensional integration: VEGAS enhanced, J. Comput. Phys. **439**, 110386 (2021).

[75] N. Aghanim *et al.*, Planck 2018 results. VI. Cosmological parameters, Astron. Astrophys. **641**, A6 (2020); **652**, C4(E) (2021).

[76] K. Saikawa and S. Shirai, Primordial gravitational waves, precisely: The role of thermodynamics in the Standard Model, J. Cosmol. Astropart. Phys. 05 035 (2018).

[77] A. Escrivà, Y. Tada, S. Yokoyama, and C.-M. Yoo, Simulation of primordial black holes with large negative non-Gaussianity, J. Cosmol. Astropart. Phys. 05 (2022) 012.

[78] A. M. Green, A. R. Liddle, K. A. Malik, and M. Sasaki, A New calculation of the mass fraction of primordial black holes, Phys. Rev. D **70**, 041502(R) (2004).

[79] T. Nakama, J. Silk, and M. Kamionkowski, Stochastic gravitational waves associated with the formation of primordial black holes, Phys. Rev. D **95**, 043511 (2017).

[80] U. Seljak and M. Zaldarriaga, A line of sight integration approach to cosmic microwave background anisotropies, Astrophys. J. **469**, 437 (1996).

[81] Y. Tada and S. Yokoyama, Primordial black holes as biased tracers, Phys. Rev. D **91**, 123534 (2015).

[82] C. R. Contaldi, Anisotropies of gravitational wave backgrounds: A line of sight approach, Phys. Lett. B **771**, 9 (2017).

[83] N. Bartolo, D. Bertacca, S. Matarrese, M. Peloso, A. Ricciardone, A. Riotto, and G. Tasinato, Anisotropies and non-gaussianity of the cosmological gravitational wave background, Phys. Rev. D **100**, 121501(R) (2019).

[84] N. Bartolo, D. Bertacca, S. Matarrese, M. Peloso, A. Ricciardone, A. Riotto, and G. Tasinato, Characterizing the cosmological gravitational wave background: Anisotropies and non-Gaussianity, Phys. Rev. D **102**, 023527 (2020).

[85] R. K. Sachs and A. M. Wolfe, Perturbations of a cosmological model and angular variations of the microwave background, Astrophys. J. **147**, 73 (1967).

[86] M. Maggiore, *Gravitational Waves: Vol. 2: Astrophysics and Cosmology* (Oxford University Press, New York, 2018).

[87] K. Schmitz, New sensitivity curves for gravitational-wave signals from cosmological phase transitions, J. High Energy Phys. 01 (2021) 097.

[88] G. Agazie *et al.*, The NANOGrav 15-year data set: Search for anisotropy in the gravitational-wave background, ApJL **956**, L3 (2023).